JOURNAL OF CHEMICAL INFORMATION AND MODELING

Article

pubs.acs.org/jcim

Molecular Dynamic Behavior and Binding Affinity of Flavonoid Analogues to the Cyclin Dependent Kinase 6/cyclin D Complex

Wasinee Khuntawee,[†] Thanyada Rungrotmongkol,[‡,*] and Supot Hannongbua[†,§]

[†]Computational Chemistry Unit Cell, Department of Chemistry, Faculty of Science, Chulalongkorn University, 254 Phayathai Road, Bangkok 10330, Thailand

[‡]Department of Biochemistry, Faculty of Science, Chulalongkorn University, 254 Phayathai Road, Bangkok 10330, Thailand

[§]Center of Excellence for Petroleum, Petrochemicals and Advanced Materials, Chulalongkorn University, 254 Phayathai Road, Bangkok 10330, Thailand

ABSTRACT: The cyclin dependent kinases (CDKs), each with their respective regulatory partner cyclin that are involved in the regulation of the cell cycle, apoptosis, and transcription, are potentially interesting targets for cancer therapy. The CDK6 complex with cyclin D (CDK6/cycD) drives cellular proliferation by phosphorylation of specific key target proteins. To understand the flavonoids that inhibit the CDK6/cycD functions, molecular dynamics simulations (MDSs) were performed on three inhibitors, fisetin (FST), apigenin (AGN), and chrysin (CHS), complexed with CDK6/cycD, including the two different binding orientations of CHS: FST-like (CHS_A) and deschloro-flavopiridol-like (CHS_B). For all three inhibitors, including both CHS orientations, the conserved interaction between the 4-keto group of the flavonoid and the backbone V101 nitrogen of CDK6 was strongly detected. The 3′- and 4′-OH groups on the flavonoid phenyl ring and the 3-OH group on the benzopyranone ring of inhibitor were found to significantly increase the binding and inhibitory efficiency. Besides the electrostatic interactions, especially through hydrogen bond formation, the van der Waals (vdW) interactions with the I19, V27, F98, H100, and L152 residues of CDK6 are also important factors in the binding efficiency of flavonoids against the CDK6/cycD complex. On the basis of the docking calculation and MM-PBSA method, the order of the predicted inhibitory affinities of these three inhibitors toward the CDK6/cycD was FST > AGN > CHS, which is in good agreement with the experimental data. In addition, CHS preferentially binds to the active CDK6 in a different orientation to FST and AGN but similar to its related analog, deschloro-flavopiridol. The obtained results are useful as the basic information for the further design of potent anticancer drugs specifically targeting the CDK6 enzyme.

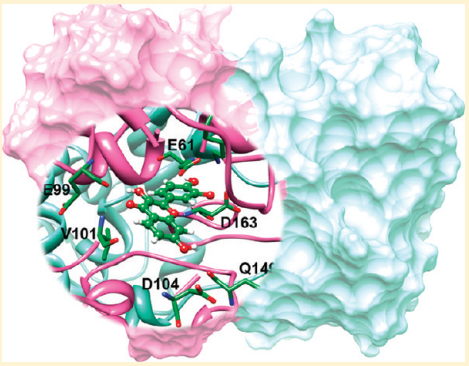

INTRODUCTION

Cancer is a foremost cause of deaths worldwide. For example, cancer accounted for around 13% of all deaths (7.6 million) in 2008.[1] Nowadays, many categories of commercial anticancer drugs targeted at DNA replication and chromosome segregation to stop cell division[2−4] have been found to show negative side effects on normal cells. Therefore, the development of a highly efficient cancer therapy with decreased toxicity is desirable. To discover new pathways that can remedy these problems, the cyclin dependent kinase type 6 (CDK6) activated by cyclin D (cycD) that drives cellular proliferation, at least in hematopoietic stem cells and tissues at the beginning of the cell cycle (G_0-G_1 and G_1-S progression), is an attractive target for both experimental and theoretical studies. Understanding at the molecular level of the particular interactions between flavonoid compounds and the CDK6/cycD complex could provide fundamental information to assist in further design and development of new potent anticancer agents.

The CDKs are a group of serine/threonine kinases that are involved in the regulation of the cell cycle, neuronal function, transcription, and apoptosis.[5,6] There are 13 known CDK family members,[7−11] and they become active only in association with a regulatory partner, cyclin. CDK6 is regulated by D-type cyclins (cyclin D1, D2, and D3) and drives cell division by phosphorylation of key proteins involved in the cell cycle, such as the retinoblastoma protein pRB and pRB-associated pocket-proteins p107 and p130. The CDK6/cycD complex regulates from the resting phase, G_0, where the cell has left the cycle and has stopped dividing, to the G1 phase cell, where it is preparing for DNA synthesis in the S phase.[12−16] In addition, it is likely to directly and indirectly, via activation of CDK2/cycE complexes, to be involved in G1 to S progression as well. In the latter case, this is mediated, at least in part, by sequestering of the cell cycle inhibitors $p27^{Kip1}$ and $p21^{Cip1}$ away from the CDK2/cycE complex. Currently, there are many categories of CDK6 inhibitors, including certain flavonoids with different numbers and positions of hydroxyl group substitutions, e.g., fisetin (FST), apigenin (AGN), and chrysin (CHR) in Figure 1. These inhibitors compete with ATP for binding into the ATP binding

Received: July 3, 2011
Published: December 15, 2011

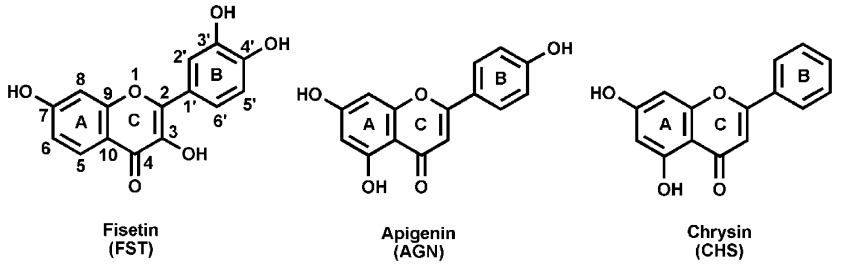

Figure 1. Chemical structures of the cyclin dependent kinase 6 (CDK6) inhibitors, fisetin (FST), apigenin (AGN), and chrysin (CHS), in which the three rings are labeled A−C.

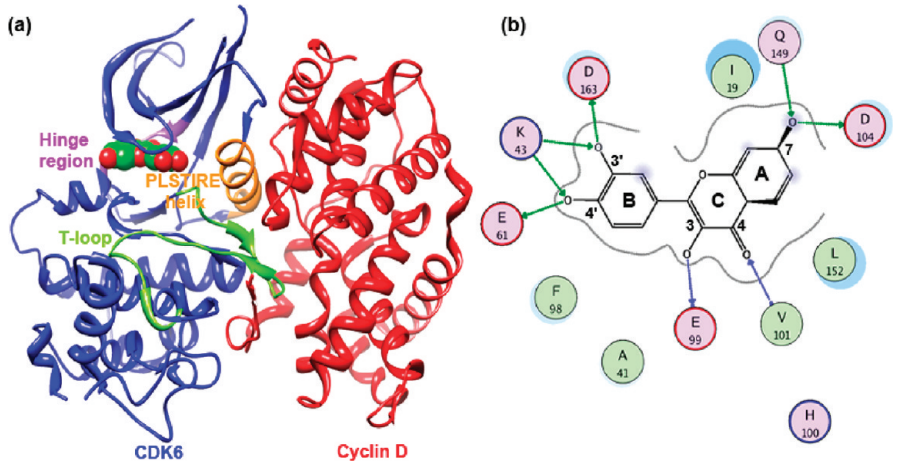

Figure 2. (a) The crystal structure of fisetin (FST), in the ATP binding site of the active CDK6 (blue) cyclin D (red) complex and the three surrounding regions, PLSTIRE helix (orange), T-loop (green), and hinge region (purple). (b) The hydrogen bonds formed between FST and the side chain and backbone of binding residues at the CDK6 active site are shown by green and blue arrows, respectively.

pocket in CDK6, and thus, the kinase activity of the CDK6/cycD complex is stopped. CDK6 separates into two domains, a β-sheet-like N-terminal domain (residues 1−100) and an α-helical-like C-terminal domain (residues 101−308). On the basis of the crystal structure of CDK6/cycD with bound FST (Figure 2a), the likely interaction of FST at the ATP-binding pocket of CDK6 is illustrated in panel (b) of Figure 2.[17] The 3′,4′-dihydroxyphenyl group (B-ring) of FST points into the ATP-binding pocket where the triphosphate of ATP would otherwise normally be located.[8] AGN is likely to bind in a related orientation, while CHS may be flipped by 180° as a result of its phenyl ring binding outward from the binding pocket, as found in the X-ray structure of deschloro-flavopiridol and the CDK2 complex.[17,18] Note that CHS is almost identical to deschloro-flavopiridol, except for that it has no piperidine ring substituent on the 8-position (Figure 1).

In order to obtain detailed information and therefore insight into the inhibitor−target interaction, structure, and dynamic properties, molecular dynamics simulations (MDSs) were performed on the three flavonoid compounds, FST, AGN, and CHS, binding to CDK6/cycD at the ATP-binding pocket. Note that these selected compounds are similar in structure and show high inhibitory activity against the target protein complex. For CHS, the two different orientations, FST-like (CHS_A) and deschloro-flavopiridol-like (CHS_B), were investigated and compared. The intermolecular hydrogen bonds, decomposition free energy and its components, and the binding free energy of the complex were all extensively analyzed.

MATERIALS AND METHODS

System Preparation. The focus-simulated systems of CDK6/cycD complexed with the three inhibitors, FST, AGN, and CHS (oriented in two binding conformations), were prepared. The initial structure of the FST−CDK6/cycD complex was taken from the Protein Data Bank (PDB), entry code 1XO2. To construct the initial structure of the other two inhibitors in the CDK6/cycD complex, the atomic coordinates of the FST in the FST−CDK6/cycD complex were separately modified to get the AGN−CDK6/cycD and CHS_A−CDK6/cycD complexes. For the CHS in the deschloro-flavopiridol-like orientation (CHS_B), the CHS_B−CDK6/cycD structure was obtained by docking procedure using the FlexibleDocking module in the Discovery Studio 2.5 (Accerys, Inc.).

The starting structure preparation and MDSs were performed using the AMBER 10 software package[19] with the ff03 force field.[20] The LEaP module was used to correct all missing hydrogen atoms of the protein and respective flavonoid ligand. The ionizable side chains of amino acids, K, R, D, and E, were defined at physiological pH. For H residues, a neutral charge with monoprotonation on the δ-nitrogen atom was given to all residues, excluding the protonated H73 and H297 residues, which have +1 charge. To reduce bad steric interactions, the hydrogen atoms were only minimized with 1000 steps of steepest descent (SD), continued by 500 steps of conjugated gradient (CG). Then, each system was solvated by TIP3P waters,[21] with a minimum distance of 10 Å from the protein surface. As a result, the water box size of all systems was 98 × 88 × 83 Å^3, while the total number of atoms were 59108, 59107, 59106, and 59109 for the FST−, AGN−, CHS_A−, and

dx.doi.org/10.1021/ci200304v | J. Chem. Inf. Model. 2012, 52, 76−83

CHS_B−CDK6/cycD complexes, respectively. A total charge of −3 was achieved for all systems and was consequently neutralized by adding three Na^+ ions. The SD (2000 steps) and CG (1000 steps) minimizations were carried out on the water molecules alone and subsequently on the whole system with the same minimization procedure to obtain the starting structures for MDS in the next step.

Force Field Development for Inhibitor Parameters. The empirical force field parameters of the three inhibitors were developed according to the standard procedure.[22−24] The hydrogen atoms were added to the inhibitor atomic coordinates by consideration of the hybridization of the covalent bonds. Using the Gaussian 03 program,[25] structure optimization with the HF/6-31* basic set was performed to adjust the ligand bond lengths and bond angles. The optimized geometry was then used to calculate the HF/6-31G* electrostatic potential (ESP) surrounding the inhibitor molecule. The restrained electrostatic potential (RESP) charges were finally obtained with the charge-fitting procedure using the RESP module of AMBER. The missing bonded parameters for each inhibitor were gained from the generalized AMBER force field (GAFF),[26] while the standard van der Waals (vdW) parameters were used to sufficient transferability of intermolecules.

Molecular Dynamics Simulations (MDSs). All MDSs were performed using the SANDER module in AMBER. The periodic boundary with NPT ensemble at 1 atm was applied. The SHAKE algorithm[27] was used to constrain all bonds involving hydrogen atoms with a time step of 2 fs being used. The cutoff distance for nonbonded interactions was set at 12 Å, and the particle mesh Ewald method[28] was applied for an adequate treatment of long-range electrostatic interactions. The whole system was heated to 298 K for 60 ps and subsequently simulated at 298 K for equilibration and production phases. All systems were well equilibrated at 6 ns, and the MDSs were prolonged for another 14 ns in all systems. For the analyses, the MD trajectories were extracted from the production phase of the last 14 ns.

The stability of the system was monitored through the convergences of energy, temperature, and global root mean-square displacement (rmsd). The ptraj and MM-PBSA modules in the AMBER software were used to analyze the rmsd, hydrogen bond occupancy between inhibitor and protein, decomposition of free energies per residue ($\Delta G_{bind}^{residue}$), and total binding free energies (ΔG_{bind}) as well as their energy components.

RESULTS AND DISCUSSION

The three focused flavonoids inhibitors, fisetin (FST), apigenin (AGN), and chrysin (CHS), are separately docked into the ATP binding site of the CDK6/cycD complex using the FlexibleDocking module in Discovery Studio 2.5. On the basis of 100 independent runs, the docked energy and conformation resulted are summarized in Table 1.

It is clear that the docking energy calculated approaches provide the same order of inhibitory affinity (FST > AGN > CHS) in good agreement with the experimental IC_{50} values. Moreover, the CHS in deschloro-flavopiridol-like form (−39.3 kcal/mol) preferentially binds to the CDK6/cycD complex rather than the CHS in fisetin-like form (−35.7 kcal/mol). To investigate the inhibitor−protein interaction and binding affinity in aqueous solution, the molecular dynamics simulation was then performed on the four complexes; the results are discussed in the following sections.

Table 1. Docked Energy and Conformation of Flavonoid Compounds against CDK6/cycD Relative to the Experimental IC_{50}[17]

compound	IC_{50} (μM)	docked energy (kcal/mol)	% docked conformation
FST	0.85	−48.2	100%, same as in X-ray structure
AGN	1.70	−41.8	100% FST-like
CHS	6.00	−35.7	38% FST-like (CHS_A)
		−39.3	62% deschloro-flavopiridol-like (CHS_B)

System Stability. The stability of the four systems was determined by rmsd analysis of the MD trajectories obtained from simulations with respect to the initial structure. The results are plotted and compared in Figure 3. The RMSDs for

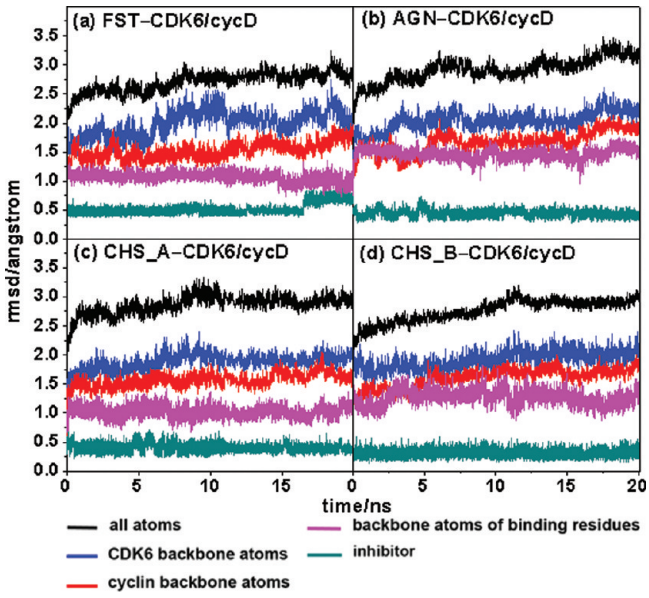

Figure 3. Plots of rmsd for the four simulated systems of (a) FST−, (b) AGN−, (c) CHS_A−, and (d) CHS_B−CDK6/cycD.

overall atoms, backbone atoms of CDK6 and cycD, flavonoid inhibitors, and backbone atoms of the residues within a 7 Å sphere of the inhibitor are shown separately.

In all systems, the rmsd of the CDK6 backbone atoms (blue in Figure 3, see also Figure 2a for the 3D structure) are relatively higher than those of the cyclin backbone atoms (red). While the rmsd fluctuations demonstrated the flexibility of the two proteins, the rmsd plots for both the inhibitor (green) and the backbone atoms of its binding residues (pink) tended to be steady along the simulation time. Taken altogether with the rmsd for the atoms (black), all complexes were likely to reach equilibrium at 6 ns. Thus, the MD trajectories from the last 14 ns simulation of all systems were taken for analysis.

Prior to focusing on the ATP binding site, the flexibility of the three surrounding regions, T-loop, hinge region, and PLSTIRE helix, are considered (Figure 2a). The MD trajectories extracted every 1 ns after the equilibrium state are superimposed and are shown in Figure 4. It is shown that these regions for all simulations are highly stable, except for the PLSTIRE helix of the CHS_A system.

Inhibitor Binding Pattern in Active CDK6. All three inhibitors studied here are classified as flavonoids but contain a different number of hydroxyl group substitutions on the three

dx.doi.org/10.1021/ci200304v | J. Chem. Inf. Model. 2012, 52, 76−83

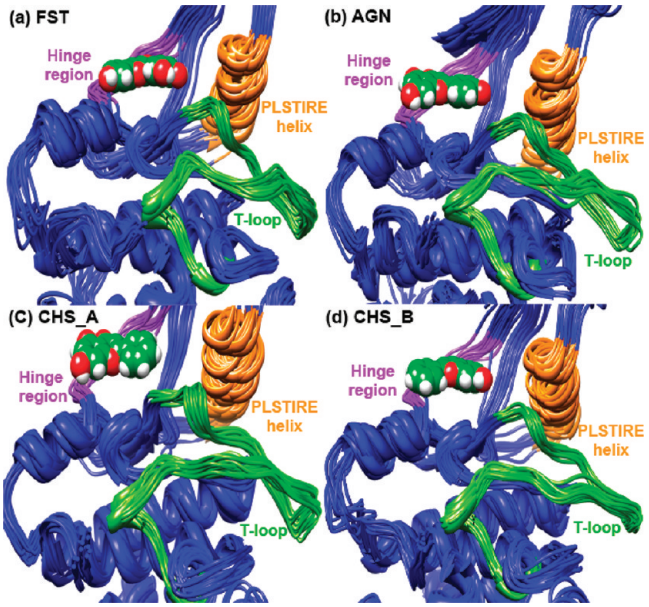

Figure 4. Closed-up of the T-loop (green), hinge region (purple), and PLSTIRE helix (orange) of the four studied systems taken from the last 14 ns simulation.

phenyl rings A−C, as shown in Figure 1. Hydrogen bonding between these hydroxyl groups as well as the carbonyl oxygen of these flavonoids and the surrounding residues is an important factor in the inhibitor binding at the active site. To monitor such interactions, the percentage and number of hydrogen bonds were calculated according to the following two criteria: (i) a proton donor−acceptor distance ≤3.5 Å, and (ii) a donor−H−acceptor bond angle ≥120°. The results are summarized in Figure 5, where the strong and medium hydrogen bond interactions are defined as having H-bond occupations of >75% and 50−75%, respectively.

As shown in Figure 5, ligand−enzyme interactions in term of the number and H-bond occupation in the four complexes were found to be in the following order: FST− > AGN− > CHS_B− > CHS_A−CDK6/cycD. The total number of strong H-bonds formed between the inhibitor and the binding residues were 4, 3, 2, and 1 for FST−, AGN−, CHS_B−, and CHS_A−CDK6/cycD complexes, respectively, and 5, 3, 2, and 1 for moderate to high, respectively. The conserved H-bonds were formed at the A- and C-rings of the inhibitor. In the A-ring, the H-bond at the 7-OH group with the $-COO^-$ group of the CDK6 D104 residue in the C-terminal domain was detected in all systems with the FST-like form (Figure 5a−c). The interaction strengths varied from rather weak H-bond in the FST− and CHS_A−CDK6/cycD systems to relatively strong H-bond in the AGN−CDK6/cycD system. This is slightly different from the crystal structure of the FST−CDK6/cycD complex, where the 7-OH oxygen of the FST also formed a hydrogen bond with the amide group of the Q149 residue of CDK6 (Figure 2b). For the CHS_B−CDK6/cycD complex, the orientation of the CHS in the CDK6 active site was flipped by 180°; so CHS_B was found to form a strong H-bond with the positively charged K43 residue of CDK6 instead. The other conserved strong H-bond interaction at the C-ring, between the 4-keto group of each of the respective flavonoid inhibitors and the backbone nitrogen of the V101 residue of CDK6, was observed in all four systems.

Accordingly, the rest of the strong or medium H-bond occur on the 5-OH group in the A-ring, the 3′- and 4′-OH groups in the B-ring, and the 3-OH group in the C-ring and are supposed to play a role in increasing the inhibitory activity of the flavonoids. In the A-ring, the addition of the −OH group at the 5-position in the AGN and CHS inhibitors has no discernible effect on the inhibitor binding at the CDK6 active site, *i.e.*, no H-bond was detected in Figures 5b−d relative to those in Figure 5a. Interestingly, the presence of the 3-OH group in the C-ring in FST induced one more strong H-bond, that being with the backbone carbonyl oxygen of CDK6 E99 (Figure 5a). Formation of this H-bond makes the FST oriented and anchored well in the hinge region between the N- and C-terminal domains of the CDK6 protein kinase, which is consistent with that found in the X-ray structure (Figure 2b). For the dihydroxylphenyl ring of FST (B-ring in Figure 5a), the

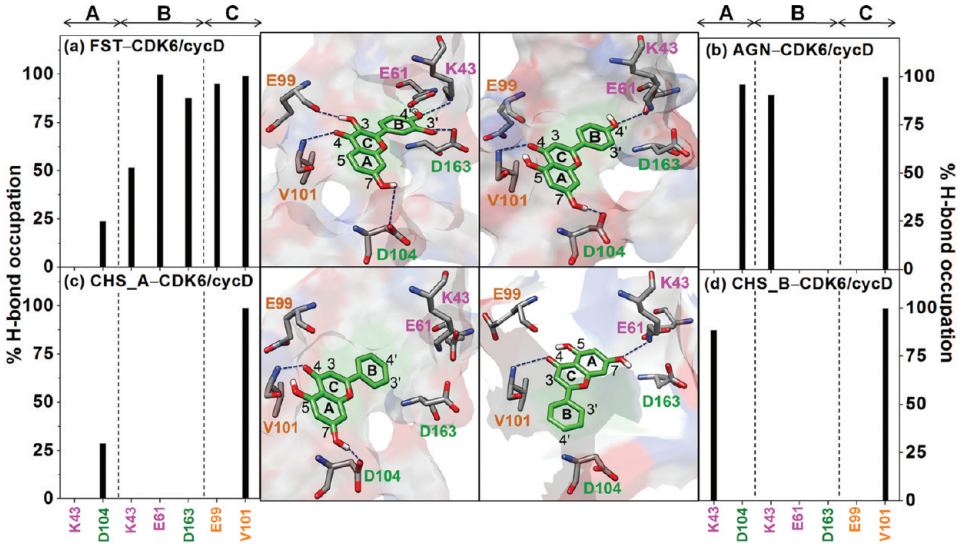

Figure 5. Percent occupation of hydrogen bonds between the CDK6 residues and inhibitor at three moieties for (a) FST−, (b) AGN−, (c) CHS_A−, and (d) CHS_B−CDK6/cycD complexes with schematic view of the flavonoid inhibitor−CDK6/cycD interactions taken from the MD snapshot.

dx.doi.org/10.1021/ci200304v | *J. Chem. Inf. Model.* 2012, 52, 76−83

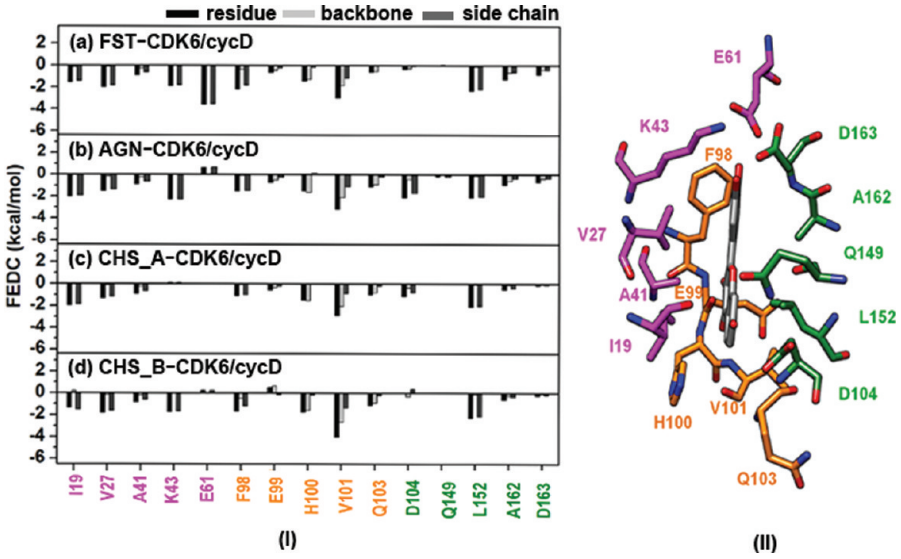

Figure 6. (I) Decomposition of the free energy on a per residue basis ($\Delta G_{bind}^{residue}$) of residues in the N-terminal domain (violet), hinge region (orange), and C-terminal domain (green) into the contributions from the atom groups of the backbone (light gray) and side chain (dark gray) in (a) FST, (b) AGN, (c) CHS_A, and (d) CHS_B bound to the CDK6/cycD complex. (II) The position of the residues in the three domains is schematically shown.

H-bonds from the 3′ and 4′-OH groups to the $-COO^-$ group of residues D163 and E61 in the C- and N-terminal domains, respectively, with occupations of ∼100%, were found to contribute considerably to the inhibitory activity of the FST. In addition, the $-NH_3^+$ moiety of K43, the residue in the N-terminal domain interacted via moderate strength hydrogen bonds with the 4′-OH group of FST. This is somewhat different than the X-ray structure of the CDK6/cycD-FST complex, where the K43 side chain was found to stabilize both −OH groups via an additional H-bond between the K43 and 3′-OH group. In panel (b) of Figure 5, the B-ring without the −OH group at the 3′-position in AGN showed significantly reduced H-bond interactions, with only a strong hydrogen bond being established from the 4′-OH group to the $-NH_3$ group of K43 and, as expected, no H-bond formation between the highly hydrophobic phenyl ring of CHS in both orientations (Figure 5c−d). It is worth noting that the important interactions with the three catalytic residues of the CDK6 protein kinase, E61, E99, and D163, were only maintained in the FST−CDK6/cycD simulation.

Per Residue Inhibitor−Enzyme Interactions. To explore the key binding motif of the flavonoid compounds inhibiting the CDK6/cycD complex, the intermolecular interactions contributed from the protein residues in contact with each inhibitor were determined in terms of the pair interaction decomposition of free energy. The calculation was performed over the last 14 ns MD snapshots using the decomposition energy module in AMBER, where more details of the pair interaction decomposition of free energy have been described in previous works.[29−31] The per residue total binding free energy ($\Delta G_{bind}^{residue}$) and the contributions from backbone atoms ($\Delta G_{bind}^{backbone}$) and side chain atoms ($\Delta G_{bind}^{side\ chain}$) of the 15 residues located in the N-terminal domain (violet), the hinge region (orange), and the C-terminal domain (green) are summarized in Figure 6. In addition, the electrostatic (E_{ele} + G_{polar}) and vdW (E_{vdW} + $G_{nonpolar}$) energy terms of each residue were also evaluated and compared in Figure 7.

Almost all of the inhibitor contacted residues provided a degree of stabilization through their side chains, where the

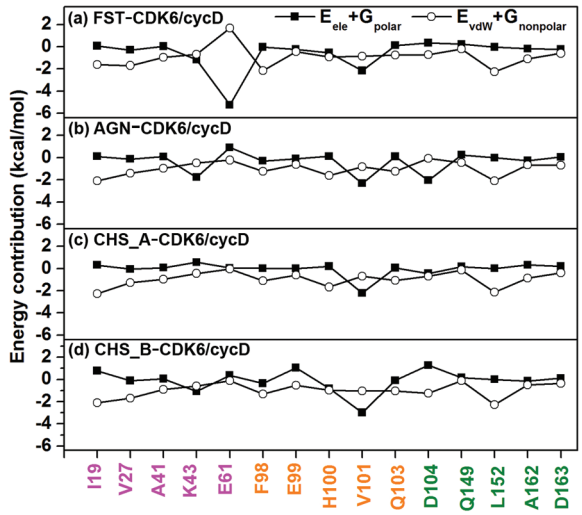

Figure 7. Energy contribution of the electrostatic (E_{ele} + G_{polar}) and vdW (E_{vdW} + $G_{nonpolar}$) interaction terms for the residues in the N-terminal domain (violet), hinge region (orange), and C-terminal domain (green) of the CDK6/cycD complex with the inhibitors (a) FST, (b) AGN, (c) CHS_A, and (d) CHS_B.

$\Delta G_{bind}^{residue}$ is almost totally contributed from the $\Delta G_{bind}^{side\ chain}$ (Figure 6). This is except for the four CDK6 residues 99−101 and 103 in the hinge region where the $\Delta G_{bind}^{backbone}$ plays a stronger role. In the N-terminal domain, the hydrophobic CDK6 side chains of residues I19, V27, and A41 created favorable vdW contacts with the respective flavonoid inhibitor molecules (Figures 6 and 7), while the positively and negatively charged side chains of K43 (for FST−, AGN−, and CHS_B−CDK6/cycD systems) and E61 (for the FST system) stabilized the inhibitor by providing an electrostatic contribution via hydrogen bond formation. The residue V101 in the hinge region provided the highest degree of stabilization ($\Delta G_{bind}^{residue}$ ≤ −3 kcal/mol) among the 15 residues for all three inhibitors, including both orientations of CHS, through its backbone ($\Delta G_{bind}^{backbone}$ ≤ −2 kcal/mol) forming a strong hydrogen

dx.doi.org/10.1021/ci200304v | J. Chem. Inf. Model. 2012, 52, 76−83

Table 2. Binding Free Energy (kcal/mol) and Its Components for the Three Kinase Inhibitors (FST, AGN, and CHS) in FST−, AGN−, CHS_A, and CHS_B−CDK6/cycD Complexes[a]

	FST−CDK6/cycD	AGN−CDK6/cycD	CHS_A−CDK6/cycD	CHS_B−CDK6/cycD
ΔE_{ele}	−56.6 ± 9.4	−45.4 ± 3.6	−25.0 ± 8.8	−26.5 ± 4.7
ΔE_{vdw}	−33.6 ± 3.0	−36.8 ± 3.1	−33.3 ± 2.3	−36.3 ± 2.2
ΔE_{MM}	−90.2.1 ± 8.9	−82.2 ± 4.1	−58.3 ± 8.2	−62.8 ± 4.7
$\Delta G_{sol}^{nonpolar}$	−4.9 ± 0.5	−4.5 ± 0.1	−4.5 ± 0.5	−4.6 ± 0.3
ΔG_{sol}^{ele}	63.2 ± 7.8	58.0 ± 3.4	41.4 ± 6.6	43.3 ± 4.1
ΔG_{sol}	56.6 ± 7.2	53.5 ± 3.4	37.0 ± 6.6	38.7 ± 4.1
$\Delta G_{sol}^{ele} + \Delta E_{ele}$	8.4 ± 5.0	12.6 ± 3.5	16.5 ± 7.7	16.8 ± 4.4
$\Delta G_{sol}^{nonpolar} + \Delta E_{vdw}$	−39.0 ± 1.7	−41.3 ± 1.6	−37.8 ± 1.4	−40.8 ± 1.3
ΔG_{bind}	−31.8 ± 4.5	−28.7 ± 2.7	−21.3 ± 4.5	−24.1 ± 4.5
IC_{50} (μM)	0.85	1.70	6.00	

[a]For comparison, the experimental IC_{50} values, taken from ref 17, are also shown.

bond with the inhibitor keto group as mentioned previously. This is supported by the energy contribution of this residue primarily from the electrostatic term of ≤ −2 kcal/mol (Figure 7). In contrast, the other four residues in this region partially built up the hydrophobic pocket for the inhibitor, as shown by the higher level of stabilizing vdW contributions in Figure 7. In the C-terminal domain, the L152 stabilization of −2 kcal/mol was found in all systems (Figure 6) and was mainly contributed from its hydrophobic side chain with favorable vdW interactions to the benzopyran ring of each respective flavonoid inhibitor. The electrostatic stabilization from D104 was dominantly observed in the AGN−CDK6/cycD system (Figures 6 and 7) due to the firmly formed strong hydrogen bond with the $-COO^-$ group (Figure 5b).

In summary, the order of per residue energy contribution from the surrounding residues to inhibitor was FST− > AGN− > CHR_A− ∼ CHS_B−CDK6/cycD. The stabilizations were achieved from both electrostatic (hydrogen bond) and vdW components from the surrounding residues.

Binding Free Energy (MM-PBSA). The MM-PBSA approach is an acceptable method in the AMBER package to evaluate the free energies of binding or to estimate the absolute free energies of molecules in solution.[32,33] The MM-PBSA free energy calculation was performed using the MM-PBSA module in the AMBER 10 software for all four flavanoid−CDK6/cycD systems using the same set of snapshots as those used to evaluate the per residue energy decomposition. The so obtained binding free energy (ΔG_{bind}) and the details of the energy contributions are summarized in Table 2.

In the gas phase (MM interaction energy), the order of the preferential favorable ΔE_{ele} contribution was FST− > AGN− > CHS_B− ∼ CHS_A−CDK6/cycD, in which the corresponding ΔE_{ele} values are −56.6, −45.4, −26.5, and −25.0 kcal/mol, respectively. This is consistent with the order of the number and percentage of hydrogen bond formations. By taking into account the solvation free energy, the polar ($\Delta G_{sol}^{ele} + \Delta E_{ele}$) energy becomes unfavorable (8.4, 12.6, 16.8, and 16.5 kcal/mol for the FST−, AGN−, CHS_B−, and CHS_A−CDK6/cycD complexes, respectively), which is determined to a large extent by the desolvation energy. This phenomenon has been also observed in some biological systems in solution.[34,35] In contrast, the ΔE_{vdW} contribution was found to be favorable with a similar value for all four flavonoid−CDK6/cycD systems (ca. from −33 to −37 kcal/mol), and therefore the nonpolar ($\Delta G_{sol}^{nonpolar} + \Delta E_{vdW}$) energy term after considering the solvation term showed more favorable contributions (−39.0, −41.3, −40.8, and −37.8 kcal/mol for the FST−, AGN−, CHS_B−, and CHS_A−CDK6/cycD complexes, respectively).

Taking into account the overall summation of the energy components, the predicted binding free energies (ΔG_{bind}) of −31.8, −28.7, −24.1, and −21.3 kcal/mol obtained for the FST−, AGN−, CHS_B−, and CHS_A−CDK6/cycD systems, respectively, were in the same order as the experimentally determined inhibitory affinities (IC_{50}). Moreover, the calculated ΔG_{bind} values suggest that CHS in the B orientation fits and binds into the ATP binding site of the active CDK6 better than CHS in the A orientation. The structural features responsible for flipping the orientation of the CHS can be explained by Figure 8. The A-ring preferentially occupies in the hydrophilic pocket established by the three charged residues, K43, E61, and D163, while the phenyl ring favorably positions in the hydrophobic pocket formed by the nonpolar side chains of I19, V101, and L152 and backbones of H100 and Q103. This is in consistent with the X-ray structure of the related analog, deschloro-flavopiridol, inhibiting the CDK2.[18]

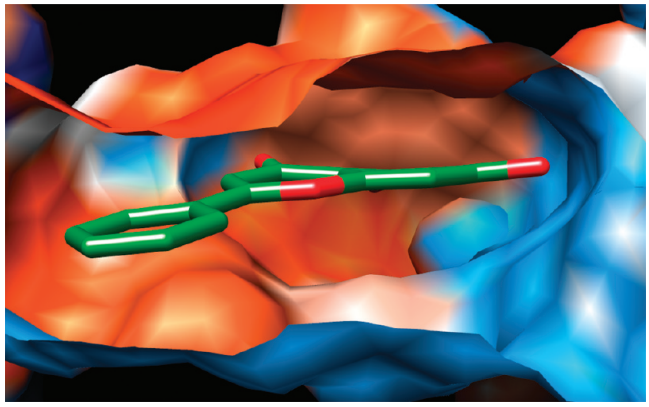

Figure 8. The chrysin in deschloro-flavopiridol-like orientation (CHS_B) in the ATP binding pocket of the CDK6 protein where the blue and orange colors represent hydrophilic and hydrophobic surfaces, respectively.

CONCLUSIONS

In this study, MDSs were applied to seek detailed information on the key intermolecular interactions and dynamic properties of the three flavonoid inhibitors, FST, AGN, and CHS, binding to the CDK6/cycD complex. The two different orientations of CHS in the ATP binding pocket of CDK6, CHS_A and CHS_B were both evaluated. Both electrostatic, especially

dx.doi.org/10.1021/ci200304v | J. Chem. Inf. Model. 2012, 52, 76−83

through hydrogen bond formation, and vdW interactions were found to be likely important factors in the binding efficiency of these three different flavonoids against the CDK6/cycD complex. The flavonoid binding strength likely depends on the number and position of the hydroxyl group substitutions as well as their orientation in the ATP binding pocket. The interaction of the carbonyl group of the respective flavonoid inhibitor with the CDK6 V101 residue is considerably conserved in all three flavonoids, including both the A and B binding conformation of CHS. The hydrogen bonds between the 7-OH group and the CDK6 D104 residue only present in the inhibitor−CDK6/cycD complexes, where the ligand is oriented in the FST-like form. Instead, the 180 degree flip in the inhibitor orientation of CHS_B leads to a strong binding interaction with K43. Interestingly, the 3′- and 4′-OH groups on the B-ring and the 3-OH group on the C-ring of FST were found to significantly increase the binding and inhibitory efficiency. In addition, the vdW interactions with the CDK6 I19, V27, F98, H100, and L152 residues located in the N-terminal domain, the hinge region, and the C-terminal domain are also important factors in the binding efficiency of flavonoids against the CDK6/cycD complex. On the basis of the MM-PBSA method and docking calculation, the order of the predicted inhibitory affinities of these three flavonoids toward the active CDK6 were the same as that of the experimentally determined IC_{50} values, *i.e.*, FST > AGN > CHS. In addition, CHS preferentially binds to the active CDK6 in a different orientation to FST and AGN, *i.e.*, similar to its related analog, deschloro-flavopiridol, which was previously found in the CDK2 crystal structure. The obtained results are useful as the basic information for the further design of potent anticancer drugs specifically targeting the CDK6 enzyme. For CDK6/cycD bound with the FST-like form, the 7-position on the A-ring might be replaced by the methyl amine group to establish the salt bridge interaction with D104, while the introduction of the acetamide group at the 4′-position on the B-ring is possible to induce the stronger hydrogen bonds with the K43 and E61.

AUTHOR INFORMATION

Corresponding Author

*Tel: +6622185426. Fax: +6622185418. E-mail: t.rungrotmongkol@gmail.com.

ACKNOWLEDGMENTS

This work was supported by the Higher Education Research Promotion and National Research University Project of Thailand, Office of the Higher Education Commission (HR1155A), and the Thai Government Stimulus Package 2 (TKK2555) under the Project for Establishment of Comprehensive Center for Innovative Food, Health Products, and Agriculture. The Center of Excellence for Petroleum, Petrochemicals, and Advanced Materials, Chulalongkorn University is acknowledged.

REFERENCES

(1) Jemal, A.; Bray, F.; Center, M. M.; Ferlay, J.; Ward, E.; Forman, D. Global cancer statistics. *Ca-Cancer J. Clin.* **2011**, *61*, 69−90.
(2) Krakoff, I. H. Cancer chemotherapeutic agents. *Ca-Cancer J. Clin.* **1977**, *27*, 130−143.
(3) Topcu, Z. DNA topoisomerases as targets for anticancer drugs. *J. Clin. Pharm. Ther.* **2001**, *26*, 405−416.
(4) Ren, J.; Singh, B. N.; Huang, Q.; Li, Z.; Gao, Y.; Mishra, P.; Hwa, Y. L.; Li, J.; Dowdy, S. C.; Jiang, S. W. DNA hypermethylation as a chemotherapy target. *Cell. Signalling* **2011**, *23*, 1082−1093.
(5) Harper, J. W.; Adams, P. D. Cyclin-dependent kinases. *Chem. Rev.* **2001**, *101*, 2511−2526.
(6) Doree, M.; Galas, S. The cyclin-dependent protein kinases and the control of cell division. *FASEB J.* **1994**, *8*, 1114−1121.
(7) Morgan, D. O. Cyclin-dependent kinases: Engines, clocks, and microprocessors. *Annu. Rev. Cell Dev. Biol.* **1997**, *13*, 261−291.
(8) Jeffrey, P. D.; Ruso, A. A.; Polyak, K.; Gibbs, E.; Hurwitz, J.; Massague, J.; Pavletich, N. P. Mechanism of CDK activation revealed by the structure of a cyclinA-CDK2 complex. *Nature* **1995**, *376*, 313−320.
(9) William, G. D. The decision to enter mitosis. *Trends Cell Biol.* **1994**, *4*, 202−207.
(10) Hoffmann, I.; Karsenti, E. The role of cdc25 in checkpoints and feedback controls in the eukaryotic cell-cycle. *J. Cell Sci.* **1994**, *18*, 75−79.
(11) Hochegger, H.; Takeda, S.; Hunt, T. Cyclin-dependent kinases and cell-cycle transitions: Does one fit all? *Nat. Rev. Mol. Cell Biol.* **2008**, *9*, 910−916.
(12) Garrett, M. A. Cell cycle control and cancer. *Curr. Sci.* **2001**, *81*, 515−522.
(13) Lew, D. J.; Kornbluth, S. Regulatory roles of cyclin dependent kinase phosphorylation in cell cycle control. *Curr. Opin. Cell Biol.* **1996**, *8* (6), 795−804.
(14) Nigg, E. A. Targets of cyclin-dependent protein kinases. *Curr. Opin. Cell Biol.* **1993**, *5*, 187−193.
(15) Vermeulen, K.; Van Bockstaele, D. R.; Berneman, Z. N. The cell cycle: A review of regulation, deregulation and therapeutic targets in cancer. *Cell Proliferation* **2003**, *36* (3), 131−149.
(16) de Cárcer, G.; Pérez de Castro, I.; Malumbres, M. Targeting cell cycle kinases for cancer therapy. *Curr. Med. Chem.* **2007**, *14*, 969−985.
(17) Lu, H. S.; Chang, D. J.; Baratte, B.; Meijer, L.; Schulze-Gahmen, U. Crystal structure of a human cyclin-dependent kinase 6 complex with a flavonol inhibitor, fisetin. *J. Med. Chem.* **2005**, *48*, 737−743.
(18) deAzevedo, W. F.; MuellerDieckmann, H. J.; SchulzeGahmen, U.; Worland, P. J.; Sausville, E.; Kim, S. H. Structural basis for specificity and potency of a flavonoid inhibitor of human CDK2, a cell cycle kinase. *Proc. Natl. Acad. Sci. U.S.A.* **1996**, *93*, 2735−2740.
(19) Case, D. A.; Darden, T. A.; Cheatham, T. E., III; Simmerling, C. L.; Wang, J.; Duke, R. E.; Luo, R.; Crowley, M.; Walker, R. C.; Zhang, W.; Merz, K. M.; Wang, B.; Hayik, S.; Roitberg, A.; Seabra, G.; Kolossváry, I.; Wong, K. F.; Paesani, F.; Vanicek, J.; Wu, X.; Brozell, S. R.; Steinbrecher, T.; Gohlke, H.; Yang, L.; Tan, C.; Mongan, J.; Hornak, V.; Mathews, G. C. D. H.; Seetin, M. G.; Sagui, C.; Babin, V.; Kollman, P. A. *AMBER10*; University of California: San Francisco, 2008.
(20) Duan, Y.; Wu, C.; Chowdhury, S.; Lee, M. C.; Xiong, G. M.; Zhang, W.; Yang, R.; Cieplak, P.; Luo, R.; Lee, T.; Caldwell, J.; Wang, J. M.; Kollman, P. A point-charge force field for molecular mechanics simulations of proteins based on condensed-phase quantum mechanical calculations. *J. Comput. Chem.* **2003**, *24*, 1999−2012.
(21) Jorgensen, W. L.; Chandrasekhar, J.; Madura, J. D.; Impey, R. W.; Klein, M. L. Comparison of simple potential functions for simulating liquid water. *J. Chem. Phys.* **1983**, *79*, 926−935.
(22) Malaisree, M.; Rungrotmongkol, T.; Decha, P.; Intharathep, P.; Aruksakunwong, O.; Hannongbua, S. Understanding of known drug target interactions in the catalytic pocket of neuraminidase subtype N1. *Proteins: Struct., Funct., Bioinf.* **2008**, *71*, 1908−1918.
(23) Udommaneethanakit, T.; Rungrotmongkol, T.; Bren, U.; Frecer, V.; Stanislav, M. Dynamic behavior of avian influenza A virus neuraminidase subtype H5N1 in complex with oseltamivir, zanamivir, peramivir, and their phosphonate analogues. *J. Chem. Inf. Model.* **2009**, *49*, 2323−2332.
(24) Arsawang, U.; Saengsawang, O.; Rungrotmongkol, T.; Sornmee, P.; Wittayanarakul, K.; Remsungnen, T.; Hannongbua, S. How do carbon nanotubes serve as carriers for gemcitabine transport in a drug delivery system? *J. Mol. Graphics Modell.* **2011**, *29*, 591−596.

(25) Frisch, M. J.; Trucks, G. W.; Schlegel, H. B.; Scuseria, G. E.; Robb, M. A.; Cheeseman, J. R.; Montgomery, J. A., Jr.; Vreven, T.; Kudin, K. N.; Burant, J. C.; Millam, J. M.; Iyengar, S. S.; Tomasi, J.; Barone, V.; Mennucci, B.; Cossi, M.; Scalmani, G.; Rega, N.; Petersson, G. A.; Nakatsuji, H.; Hada, M.; Ehara, M.; Toyota, K.; Fukuda, R.; Hasegawa, J.; Ishida, M.; Nakajima, T.; Honda, Y.; Kitao, O.; Nakai, H.; Klene, M.; Li, X.; Knox, J. E.; Hratchian, H. P.; Cross, J. B.; Bakken, V.; Adamo, C.; Jaramillo, J.; Gomperts, R.; Stratmann, R. E.; Yazyev, O.; Austin, A. J.; Cammi, R.; Pomelli, C.; Ochterski, J. W.; Ayala, P. Y.; Morokuma, K.; Voth, G. A.; Salvador, P.; Dannenberg, J. J.; Zakrzewski, V. G.; Dapprich, S.; Daniels, A. D.; Strain, M. C.; Farkas, O.; Malick, D. K.; Rabuck, A. D.; Raghavachari, K.; Foresman, J. B.; Ortiz, J. V.; Cui, Q.; Baboul, A. G.; Clifford, S.; Cioslowski, J.; Stefanov, B. B.; Liu, G.; Liashenko, A.; Piskorz, P.; Komaromi, I.; Martin, R. L.; Fox, D. J.; Keith, T.; Al-Laham, M. A.; Peng, C. Y.; Nanayakkara, A.; Challacombe, M.; Gill, P. M. W.; Johnson, B.; Chen, W.; Wong, M. W.; Gonzalez, C.; Pople, J. A. *Gaussian 03, Revision C.02*; Gaussian, Inc.: Wallingford, CT, 2004.

(26) Wang, J. M.; Wolf, R. M.; Caldwell, J. W.; Kollman, P. A.; Case, D. A. Development and testing of a general AMBER force field. *J. Comput. Chem.* **2004**, *25*, 1157−1174.

(27) Ryckaert, J.-P.; Ciccotti, G.; Berendsen, H. J. C. Numerical integration of the cartesian equations of motion of a system with constraints: Molecular dynamics of n-alkanes. *J. Comput. Phys.* **1977**, *23*, 327−341.

(28) York, D. M.; Darden, T. A.; Pedersen, L. G. The effect of long-range electrostatic interaction in simulation of macromolecular crystals: A comparison of the Ewald and Truncated list methods. *J. Chem. Phys.* **1993**, *99*, 8345−8348.

(29) Rungrotmongkol, T.; Nunthaboot, N.; Malaisree, M.; Kaiyawet, N.; Yotmanee, P.; Meeprasert, A.; Hannongbua, S. Molecular insight into the specific binding of ADP-ribose to the nsP3 macro domains of chikungunya and venezuelan equine encephalitis viruses: Molecular dynamics simulations and free energy calculations. *J. Mol. Graphics Modell.* **2010**, *29*, 347−353.

(30) Decha, P.; Rungrotmongkol, T.; Intharathep, P.; Malaisree, M.; Aruksakunwong, O.; Laohpongspaisan, C.; Parasuk, V.; Sompornpisut, P.; Pianwanit, S.; Kokpol, S.; Hannongbua, S. Source of high pathogenicity of an avian influenza virus H5N1: Why H5 is better cleaved by furin. *Biophys. J.* **2008**, *95*, 128−134.

(31) Shen, J.; Quiocho, F. A. Calculation of binding energy differences for receptor−ligand systems using the Poisson−Boltzmann method. *J. Comput. Chem.* **1995**, *16*, 445−448.

(32) Wittayanarakul, K.; Hannongbua, S.; Feig, M. Accurate prediction of protonation state as a prerequisite for reliable MM-PB(GB)SA binding free energy calculations of HIV-1 protease inhibitors. *J. Comput. Chem.* **2008**, *29*, 673−685.

(33) Swanson, J. M. J.; Henchman, R. H.; McCammon, J. A. Revisiting free energy calculations: A theoretical connection to MM/PBSA and direct calculation of the association free energy. *Biophys. J.* **2004**, *86*, 67−74.

(34) Aruksakunwong, O.; Malaisree, M.; Decha, P.; Sompornpisut, P.; Parasuk, V.; Pianwanit, S.; Hannongbua, S. On the lower susceptibility of oseltamivir to influenza neuraminidase subtype N1 than those in N2 and N9. *Biophys. J.* **2007**, *92*, 798−807.

(35) Malaisree, M.; Rungrotmongkol, T.; Nunthaboot, N.; Aruksakunwong, O.; Intharathep, P.; Decha, P.; Sompornpisut, P.; Hannongbua, S. Source of oseltamivir resistance in avian influenza H5N1 virus with the H274Y mutation. *Amino Acids* **2009**, *37*, 725−732.